Scalable Robust Beamforming for Multi-Layer Refracting RIS-Assisted HAP-SWIPT Networks

Yifu Sun[1,2], Kang An[1], Zhi Lin[3,4], Yonggang Zhu[1], Naofal Al-Dhahir[5], and Kai-Kit Wong[6,7]
[1] The Sixty-third Research Institute, National University of Defense Technology, Nanjing, China
[2] College of Electronic Science and Technology, National University of Defense Technology, Changsha, China
[3] College of Electronic Engineering, National University of Defense Technology, Hefei, China
[4] School of Computer Science and Engineering, Macau University of Science and Technology, Macau, China
[5] Department of Electrical and Computer Engineering, The University of Texas at Dallas, Richardson, USA
[6] Department of Electronic and Electrical Engineering, University College London, London, U.K.
[7] School of Integrated Technology, Yonsei University, Seoul, South Korea
Email: sunyifu_nudt@163.com, ankang89@nudt.edu.cn, linzhi945@163.com, zhumaka1982@163.com, aldhahir@utdallas.edu, kai-kit.wong@ucl.ac.uk

***Abstract*—To mitigate the severe large-scale fading and the energy scarcity problem in long-distance high-altitude platform (HAP) networks, in this paper, we investigate the potentials of a multi-layer refracting reconfigurable intelligent surface (RIS) -assisted receiver for enabling simultaneous wireless information and power transfer (SWIPT) in HAP networks. Unlike the existing RIS-aided reflector and transmitter, the multi-layer RIS-receiver can well overcome the severe "double fading" effect induced by the extreme long-distance HAP links and fully exploit RIS's degrees-of-freedom (DoFs) for SWIPT design. Building on the proposed RIS-receiver, this paper formulates a worst-case sum rate maximization problem under angular channel state information (CSI) imperfection, while satisfying the information rate requirements of the earth stations (ESs) and the harvested energy constraint. To handle the intractable non-convex problem, a scalable robust optimization framework utilizing the discretization method, LogSumExp-dual scheme, and modified cyclic coordinate descent (M-CCD) is proposed to obtain the semi-closed-form solutions. Numerical simulations demonstrate that the proposed architecture and optimization framework achieve superior performance with lower complexity compared with state-of-the-art schemes in HAP networks.**

***Index Terms*—High-altitude platform (HAP), reconfigurable intelligent surface (RIS), simultaneous wireless information and power transfer (SWIPT), scalable robust optimization.**

I. Introduction

DUE to the high elevation angles, deployment flexibility, and hybrid connectivity with multi-band radio frequencies, high-altitude platform (HAP) has emerged as an aerial base station to provide sustainable services and broad coverage for remote areas or disaster recovery [1]–[4]. However, since the battery-powered wireless devices in HAP networks are often deployed in rural, remote, and unpopulated areas, it is inconvenient or infeasible to recharge or frequently replace the limited-capacity batteries, which constitutes a serious bottleneck for HAP communications [5]. Fortunately, simultaneous wireless information and power transfer (SWIPT) can be adopted to alleviate the energy scarcity and prolong the lifetime of energy-constrained devices [6]. As one of the key techniques in SWIPT, power splitting (PS) divides the received signals into two power streams, i.e., the information stream for information decoding and the power one for energy harvesting, which brings great convenience to the deployment of energy-limited devices [6]. Although SWIPT has been widely adopted to provide a perpetual energy supply to terrestrial communications [7] and LAP communications [8], its energy transmission efficiency significantly decreases with increasing distance due to the severe large-scale fading effects. Hence, SWIPT cannot enable energy harvesting in extreme long-distance HAP communications. To our best knowledge, there are no existing works investigating HAP-SWIPT networks, which is an open and challenging research topic.

Based on the above-cited considerations, techniques which can intelligently boost communication link quality and efficiently transmit energy from HAP to the wireless devices are urgently needed. Fortunately, reconfigurable intelligent surface (RIS), as a revolutionary technique, has been proposed to manipulate the wireless channels as needed [9]. The current state-of-the-art of RIS-aided wireless communications can be divided into two main research streams. The first research stream uses RIS (passive/active) to act as a relay-like reflector for reconfiguring the EM waves propagation environment, which has been shown to increase the service coverage [9]–[11], maximize the achievable rate [12], and improve the SWIPT performance of both terrestrial and LAP communications [13], [14]. The second research stream employs RIS to act like a low-cost and power-efficient transmitter for manipulating the radiated EM waves, including a single-layer RIS-assisted transmitter [15]–[17] and a multi-layer one [18]. Nevertheless, the above RIS-aided reflectors and transmitters are not perfectly applicable to HAP-SWIPT networks. Specifically, HAP-SWIPT networks work at several dozen kilometers altitude, such that the HAP-SWIPT using RIS-reflector may suffer from

extremely severe "double fading" effect. In addition, the HAP-SWIPT networks with RIS-transmitter should consider multi-user beamforming coordination at RIS, which limits the RIS's potentials in HAP-SWIPT networks. Thus, a new RIS-aided architecture is needed to fully release the potential of HAP-SWIPT networks, which motivates this paper.

On the other hand, a well-known open issue of RIS-assisted wireless communications is the beamforming design, which involves multiple highly-coupled optimization variables [19]. To solve this intractable problem, conventional methods firstly decouple these variables into multiple subproblems, and then the multiple non-convex subproblems are relaxed into the convex ones, such that these convexified subproblems can be solved using an off-the-shelf optimization toolbox such as CVX [20]. However, the limitation in the conventional methods is that the optimization toolbox has extremely high computational complexity, especially under channel state information (CSI) imperfection [20]–[24]. Thus, this limitation calls for the design of a scalable robust beamforming design.

Motivated by the studies above, this paper first proposes a novel multi-layer refracting RIS-assisted receiver to enhance HAP-SWIPT networks by mitigating the severe "double fading" effect induced by the extreme long-distance HAP links and fully exploiting degrees-of-freedom (DoFs) for the beamforming design. Besides, we formulate a worst-case optimization problem for HAP-SWIPT. To handle the formulated intractable problem, a scalable robust optimization scheme specializing on the discretization method, LogSumExp-dual scheme, and modified cyclic coordinate descent (M-CCD) is proposed to obtain the closed-form solutions of each optimization variables, which does not rely on the off-the-shelf optimization toolbox and is beneficial to implement in practical massive large-scale array systems. Finally, numerical simulations demonstrate that the proposed architecture and optimization framework can obtain superior performance with lower complexity in comparison with the existing works.

II. System Model and Problem Formulation

A. Refracting RIS-Receiver-Aided HAP-SWIPT Networks

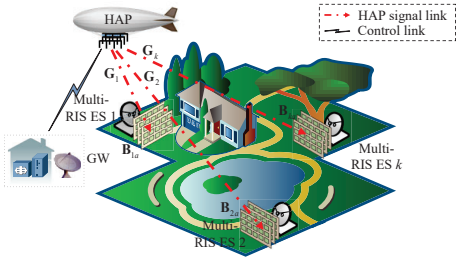

Fig. 1: System model.

Fig. 1 depicts the considered RIS-assisted HAP-SWIPT network, where a HAP equipped with $N_{\mathrm{H}}{=}N_{\mathrm{H1}} \times N_{\mathrm{H2}}$ uniform planar array (UPA) antennas transmits the desired signals to K earth stations (ESs) with the aid of the multi-layer refracting RIS-assisted receiver. At the ESs, the received signals are split for information decoding and energy harvesting. Here, the gateway acts as a control center to implement control functions [1]. We assume that the k-th ES's multi-layer refracting RIS is composed of A layers having $N_{\mathrm{E},ka}{=}N_{\mathrm{E},ka1} \times N_{\mathrm{E},ka2}$ on the a-th layer, and the k-th ES is equipped with $N_{\mathrm{D},k}$ receive (Rx) antennas for digital decoding. In addition, the channels between HAP and the k-th ES, between the a-th laye r and the $(a{+}1)$-th layer, and between the A-th layer and the k-th ES's Rx antennas are denoted as $\mathbf{G}_k \in \mathbb{C}^{N_{\mathrm{E},k1} \times N_{\mathrm{H}}}$, $\mathbf{B}_{ka} \in \mathbb{C}^{N_{\mathrm{E},k(a+1)} \times N_{\mathrm{E},ka}}$, and $\mathbf{B}_{kA} \in \mathbb{C}^{N_{\mathrm{D},k} \times N_{\mathrm{E},kA}}$, respectively.

B. Multi-Layer Refracting RIS-Assisted Receiver Model

As shown in Fig. 1, multiple refracting RISs are vertically stacked in front of the ES's Rx antennas to form a multi-layer receiver architecture, where the refracting RISs and the Rx antennas perform the analog and the digital decoding on the HAP's transmitted signals, respectively. The a-th layer's refracting coefficient matrix of the ES k is given by $\mathbf{\Xi}_{ka} = \mathrm{diag}\left(e^{j\theta_{ka,1}}, \cdots, e^{j\theta_{ka,N_{\mathrm{E},ka}}}\right) \in \mathbb{C}^{N_{\mathrm{E},ka} \times N_{\mathrm{E},ka}}$, and the k-th ES's digital processing vector is expressed as $\mathbf{v}_k \in \mathbb{C}^{N_{\mathrm{D},k} \times 1}$. Here, $\theta_{ka,n} \in [0, 2\pi)$ denotes the phase shift of the n-th RIS unit. Hence, the equivalent analog decoder generated by the k-th ES's RIS-aided receiver is given by $\mathbf{\Omega}_{k,(1,A)}$, i.e.,

$$\mathbf{\Omega}_{k,(u,v)} = \begin{cases} \prod_{a=u}^{v} \mathbf{B}_{ka}\mathbf{\Xi}_{ka}, u, v \in [A], \\ \mathbf{I}_{N_{\mathrm{E},k1}}, u = 1, v = 0, \\ \mathbf{I}_{N_{\mathrm{D},k}}, u = A+1, v = A. \end{cases} \tag{1}$$

Different from typical receiver, the proposed RIS-receiver does not entail numerous power-hungry RF components and costly phased arrays, which facilitates the deployment of a large-scale antenna array at the user side in a cost-efficient way [25].

C. Signal Transmission and Energy Harvesting Model

Denote by s_k the desired symbol transmitted by the HAP to the k-th ES, which satisfies $\mathbb{E}\left\{|s_k|^2\right\} = 1$. Prior to transmission, s_k is processed by the digital precoder $\mathbf{w}_k \in \mathbb{C}^{N_{\mathrm{H}} \times 1}$, such that the signal transmitted by the HAP is $\sum_{k=1}^{K} \mathbf{w}_k s_k$. Then, after decoding the transmitted signals by the analog and the digital decoder $\mathbf{\Omega}_{k,(1,A)}$ and $\mathbf{v}_k$, the received signal at the k-th ES can be expressed as

$$y_k = \mathbf{v}_k^H \left(\mathbf{\Omega}_{k,(1,A)}\mathbf{G}_k \sum\nolimits_{k=1}^{K} \mathbf{w}_k s_k + \mathbf{n}_k\right), \tag{2}$$

where $\mathbf{n}_k \sim \mathcal{CN}(0, \sigma_k^2 \mathbf{I}_{N_{\mathrm{D},k}})$ is the thermal noise at the k-th ES's Rx antennas. Subsequently, the k-th ES divides the received signals into two portions, where γ_k portion is utilized for information decoding and $1-\gamma_k$ one is used for energy harvesting. Hence, the k-th ES's received signals for information decoding and energy harvesting are, respectively, given by $y_{\mathrm{ID},k} = \sqrt{\gamma_k} y_k + z_k$ and $y_{\mathrm{EH},k} = \sqrt{1-\gamma_k} y_k$, where $\gamma_k \in (0, 1]$ is the PS ratio and $z_k \sim \mathcal{CN}(0, \delta_k^2)$ is the additional noise induced by the k-th ES's information decoding circuit

[14]. Thus, the achievable rate for information decoding at the k-th ES is given by

$$R_{\mathrm{ID},k}=\log_2\left(1+\frac{\left|\mathbf{g}_k^H\mathbf{w}_k\right|^2}{\sum_{i\neq k}^{K}\left|\mathbf{g}_k^H\mathbf{w}_i\right|^2+\sigma_k^2+\delta_k^2/\gamma_k}\right), \quad (3)$$

where $\mathbf{g}_k=\mathbf{G}_k^H\mathbf{\Omega}_{k,(1,A)}^H\mathbf{v}_k$.

Note that there are two major drawbacks in practical energy-harvesting circuits. First, the energy harvesting cannot be activated when the input power is less than the sensitivity power. Second, the harvested energy increases with the input power non-linearly [7]. To account for these effects, this paper adopts the nonlinear energy-harvesting model in [7]. Thus, the harvested energy at k-th ES is

$$\zeta_{\mathrm{EH},k}=(\alpha p_k+\beta)/(p_k+\varepsilon)-\beta/\varepsilon, \quad (4)$$

where $p_k=\eta_k\left(1-\gamma_k\right)\sum_{i=1}^{K}\left|\mathbf{g}_k^H\mathbf{w}_i\right|^2$ denotes the input power for energy harvesting, $\{\alpha,\beta,\varepsilon\}>0$ captures the sensitivity and saturation thresholds of the energy-harvesting circuits, and $\eta_k\in(0,1]$ is the energy conversion efficiency. Here, $\{\alpha,\beta,\varepsilon\}$ can be estimated by applying a best-fit match with experimental data [14], and η_k is set as 1 for brevity.

D. Problem Formulation

Due to the channel estimation error and feedback delay, only the imperfect angular CSI $\{\mathbf{G}_k\}$ can be obtained at the gateway [1]. To elaborate, the precise positions of ESs are unknown but the uncertainty region of the angular information can be obtained. Thus, $\{\mathbf{G}_k\}$ belongs to the given uncertainty set, i.e., $\Delta=\{\mathbf{G}_k|\,\theta_k\in[\theta_{k,\mathrm{L}},\theta_{m,\mathrm{U}}],\varphi_k\in[\varphi_{k,\mathrm{L}},\varphi_{k,\mathrm{U}}]\}$, where θ_{U} and θ_{L} denote the upper and lower bounds of azimuth angle, while φ_{U} and φ_{L} are the upper and lower bounds of elevation angle, respectively. Next, a worst-case achievable rate maximization problem is formulated, while meeting the information rate requirements of the ESs, the harvested energy requirements, the total transmit power constraints, and the RIS unit-modula constraints. Thus, the corresponding optimization problem can be formulated as

$$\max_{\mathbf{w}_k,\mathbf{\Xi}_{ka},\mathbf{v}_k,\gamma_k}\ \min_{\Delta}\sum_{k=1}^{K}R_{\mathrm{ID},k} \quad (5)$$
$$s.t.\,\mathrm{C1}:\min_{\Delta}R_{\mathrm{ID},k}\geq\Gamma_k,\forall k,\mathrm{C2}:\min_{\Delta}\zeta_{\mathrm{EH},k}\geq\varsigma_{\max},\forall k,$$
$$\mathrm{C3}:\sum_{k=1}^{K}\left\|\mathbf{w}_k\right\|^2\leq P_{\max},\mathrm{C4}:\left|[\mathbf{\Xi}_{ka}]_{n,n}\right|=1,\forall k,a,n,$$

where Γ_k is the minimum rate threshold, $\varsigma_{\max}$ denotes the harvested energy requirement, and $P_{\max}$ is the power limit at HAP. The optimization problem (5) is non-convex, thus, we propose a low-complexity scalable beamforming scheme to obtain a semi-closed-form solutions without relying on any optimization toolbox.

III. Scalable Robust Beamforming Design

A. LogSumExp-Dual Scheme for $\mathbf{w}_k$

Firstly, we focus on optimizing the transmit precoder $\mathbf{w}_k$ under the angular uncertainty Δ. By defining $\overline{\varsigma}_{\max}=\varepsilon\varsigma_{\max}/(\alpha-\varsigma_{\max}-\beta/\varepsilon)$ and $\overline{\gamma}_k=\log_2\left(\overline{\varsigma}_{\max}/(1-\gamma_k)\right)$, the subproblem for $\mathbf{w}_k$ can be expressed as

$$\max_{\mathbf{w}_k}\min_{\Delta}\sum_{k=1}^{K}R_{\mathrm{ID},k} \quad (6)$$
$$s.t.\ \mathrm{C1},\overline{\mathrm{C}}3:\sum_{k=1}^{K}\left\|\mathbf{w}_k\right\|^2=P_{\max},$$
$$\overline{\mathrm{C}}2:\min_{\Delta}R_{\mathrm{EH},k}=\log_2\left(\sum_{i=1}^{K}\left|\mathbf{g}_k^H\mathbf{w}_i\right|^2\right)\geq\overline{\gamma}_k,\forall k.$$

Note that the power constraint C3 must hold with equality when the objective function of (6) achieves the maximum, thus we transform C3 into $\overline{\mathrm{C}}3$ in this subproblem. Clearly, there still exists three major obstacles which prevent us from obtaining the semi-closed-form solution $\mathbf{w}_k$ to (6), i.e., the continuous angular uncertainty Δ, the non-convexity of the objective, and the non-smoothness of C1 and $\overline{\mathrm{C}}2$. In what follows, we overcome the foregoing obstacles step-by-step.

At first, we turn to the continuous angular uncertainty Δ with infinite possibilities. A discretization method is exploited to convert the imperfect CSI with Δ into a tractable form. To elaborate, since the available CSI belongs to a given continuous angular set, we select uniformly spaced angles as

$$\begin{aligned}\theta^{(p)}&=\theta_L+(i-1)\,\Delta\theta,\ p=1,\cdots,Q_1,\\ \varphi^{(q)}&=\varphi_L+(j-1)\,\Delta\varphi,\ q=1,\cdots,Q_2,\end{aligned} \quad (7)$$

where Q_1 and Q_2 are the number of samples of θ and φ, respectively, $\Delta\theta=(\theta_U-\theta_L)/(Q_1-1)$, and $\Delta\varphi=(\varphi_U-\varphi_L)/(Q_2-1)$. Hence, the equivalent CSI $\mathbf{g}_k$ is converted into a robust one, i.e.,

$$\widehat{\mathbf{g}}_k\widehat{\mathbf{g}}_k^H=\sum_{p=1}^{N_{\mathrm{H}1}N_{\mathrm{E}1,k1}}\sum_{q=1}^{N_{\mathrm{H}2}N_{\mathrm{E}2,k1}}\frac{1}{N_{\mathrm{H}}N_{\mathrm{E},k1}}\widehat{\mathbf{g}}_k^{(p,q)}\widehat{\mathbf{g}}_k^{(p,q),H}, \quad (8)$$

where $\widehat{\mathbf{g}}_k^{(p,q)}=\mathbf{G}_k^{(p,q),H}\mathbf{\Omega}_{k,(1,A)}^H\mathbf{v}_k$. The interested readers can refer to our previous works [1], [12], [15], [16], [18] for more details, which is omitted here for brevity. With the robust CSI, the $\min_{\Delta}$ operation in both the objective function and the constraints can be removed. Next, we handle the non-smoothness of constraints and the non-convex objective. The constraints C1 and $\overline{\mathrm{C}}2$ can be equivalently recast as

$$\widetilde{\mathrm{C}}1:\min_{\forall k\in[K]}R_{\mathrm{ID},k}\geq\Gamma_k,\widetilde{\mathrm{C}}2:\min_{\forall k\in[K]}R_{\mathrm{EH},k}\geq\overline{\gamma}_k. \quad (9)$$

Thus, the LogSumExp inequality in [26] can be adopted to approximate the non-smooth minimum function $\widetilde{\mathrm{C}}1$ and $\widetilde{\mathrm{C}}2$ as a smooth ones, which can be recast as

$$\min_{\forall k\in[K]}R_{\mathrm{ID},k}\approx-\rho\ln\left\{\sum_{k=1}^{K}\exp\left[\log_2\left(\frac{\overline{\mathbf{w}}^H\widehat{\mathbf{A}}_k\overline{\mathbf{w}}}{\overline{\mathbf{w}}^H\widehat{\mathbf{B}}_k\overline{\mathbf{w}}}\right)^{-\frac{1}{\rho}}\right]\right\}, \quad (10)$$

$$\min_{\forall k\in[K]}R_{\mathrm{EH},k}\approx-\rho\ln\left\{\sum_{k=1}^{K}\exp\left[\log_2\left(\frac{\overline{\mathbf{w}}^H\widehat{\mathbf{A}}_k\overline{\mathbf{w}}}{\overline{\mathbf{w}}^H\mathbf{C}_k\overline{\mathbf{w}}}\right)^{-\frac{1}{\rho}}\right]\right\}, \quad (11)$$

where $\rho>0$ denotes the smoothing parameter, $\overline{\mathbf{w}}=\left[\mathbf{w}_1^T,\mathbf{w}_2^T,\cdots,\mathbf{w}_K^T\right]^T\in\mathbb{C}^{KN_{\mathrm{H}}\times1}$, $\overline{\sigma}_k^2=\sigma_k^2+\delta_k^2/\gamma_k$, $\mathbf{C}_k=(1/P_{\max})\,\mathbf{I}_{KN_{\mathrm{H}}}$,

$\widehat{\mathbf{A}}_k=\mathrm{Blkdiag}\left\{\widehat{\mathbf{g}}_k\widehat{\mathbf{g}}_k^H,\cdots,\widehat{\mathbf{g}}_k\widehat{\mathbf{g}}_k^H\right\}+\left(\overline{\sigma}_k^2/P_{\max}\right)\mathbf{I}_{KN_{\mathrm{H}}}$,

$$\widehat{\mathbf{B}}_k=\widehat{\mathbf{A}}_k-\mathrm{Blkdiag}\left\{\mathbf{0}_{N_{\mathrm{H}}\times N_{\mathrm{H}}},\cdots,\underbrace{\widehat{\mathbf{g}}_k\widehat{\mathbf{g}}_k^H}_{k-\mathrm{th\ block}},\cdots,\mathbf{0}_{N_{\mathrm{H}}\times N_{\mathrm{H}}}\right\}.$$

$$\mathbf{N}\left(\overline{\mathbf{w}}\right)=\mathcal{L}_{\mathrm{num}}\left(\overline{\mathbf{w}}\right)\times\sum\nolimits_{k=1}^{K}\left\{1+\frac{\lambda\exp\left(-\frac{1}{\rho}\log_2\left(\frac{\overline{\mathbf{w}}^H\widehat{\mathbf{A}}_k\overline{\mathbf{w}}}{\overline{\mathbf{w}}^H\widehat{\mathbf{B}}_k\overline{\mathbf{w}}}\right)\right)}{\sum_{m=1}^{K}\exp\left(-\frac{1}{\rho}\log_2\left(\frac{\overline{\mathbf{w}}^H\widehat{\mathbf{A}}_m\overline{\mathbf{w}}}{\overline{\mathbf{w}}^H\widehat{\mathbf{B}}_m\overline{\mathbf{w}}}\right)\right)}+\frac{\mu\exp\left(-\frac{1}{\rho}\log_2\left(\frac{\overline{\mathbf{w}}^H\widehat{\mathbf{A}}_k\overline{\mathbf{w}}}{\overline{\mathbf{w}}^H\mathbf{C}_k\overline{\mathbf{w}}}\right)\right)}{\sum_{m=1}^{K}\exp\left(-\frac{1}{\rho}\log_2\left(\frac{\overline{\mathbf{w}}^H\widehat{\mathbf{A}}_m\overline{\mathbf{w}}}{\overline{\mathbf{w}}^H\mathbf{C}_m\overline{\mathbf{w}}}\right)\right)}\right\}\frac{\widehat{\mathbf{A}}_k}{\overline{\mathbf{w}}^H\widehat{\mathbf{A}}_k\overline{\mathbf{w}}}, \quad (16)$$

$$\mathbf{M}\left(\overline{\mathbf{w}}\right)=\mathcal{L}_{\mathrm{den}}\left(\overline{\mathbf{w}}\right)\times\sum\nolimits_{k=1}^{K}\left\{\left(1+\frac{\lambda\exp\left(-\frac{1}{\rho}\log_2\left(\frac{\overline{\mathbf{w}}^H\widehat{\mathbf{A}}_k\overline{\mathbf{w}}}{\overline{\mathbf{w}}^H\widehat{\mathbf{B}}_k\overline{\mathbf{w}}}\right)\right)}{\sum_{m=1}^{K}\exp\left(-\frac{1}{\rho}\log_2\left(\frac{\overline{\mathbf{w}}^H\widehat{\mathbf{A}}_m\overline{\mathbf{w}}}{\overline{\mathbf{w}}^H\widehat{\mathbf{B}}_m\overline{\mathbf{w}}}\right)\right)}\right)\frac{\widehat{\mathbf{B}}_k}{\overline{\mathbf{w}}^H\widehat{\mathbf{B}}_k\overline{\mathbf{w}}}+\frac{\mu\exp\left(-\frac{1}{\rho}\log_2\left(\frac{\overline{\mathbf{w}}^H\widehat{\mathbf{A}}_k\overline{\mathbf{w}}}{\overline{\mathbf{w}}^H\mathbf{C}_k\overline{\mathbf{w}}}\right)\right)}{\sum_{m=1}^{K}\exp\left(-\frac{1}{\rho}\log_2\left(\frac{\overline{\mathbf{w}}^H\widehat{\mathbf{A}}_m\overline{\mathbf{w}}}{\overline{\mathbf{w}}^H\mathbf{C}_m\overline{\mathbf{w}}}\right)\right)}\frac{\mathbf{C}_k}{\overline{\mathbf{w}}^H\mathbf{C}_k\overline{\mathbf{w}}}\right\}.$$

Note that (10) and (11) are the functions of Rayleigh quotients since both of the numerator and denominator can be be normalized by $\|\overline{\mathbf{w}}\|=\sqrt{P_{\max}}$. For this reason, the power constraint $\overline{\mathrm{C}}3$ can be ignored. Besides, $\overline{\mathrm{C}}3$ can also be guaranteed by the derived semi-closed-form solution later. Hence, problem (6) can be reformulated as

$$\max_{\overline{\mathbf{w}}}\sum\nolimits_{k=1}^{K}R_{\mathrm{ID},k}\ s.t.\ \widetilde{\mathrm{C}}1,\widetilde{\mathrm{C}}2. \quad (12)$$

Similar to [13], the optimal solution to (12) can be obtained by solving its dual problem. Hence, by adding $\widetilde{\mathrm{C}}1$ and $\widetilde{\mathrm{C}}2$ into the objective function in (6) with the non-negative Lagrange multipliers λ and μ, we have the partial Lagrangian function of problem (6), i.e.,

$$\mathcal{L}\left(\overline{\mathbf{w}},\lambda,\mu\right)=\sum\nolimits_{k=1}^{K}\log_2\left(\frac{\overline{\mathbf{w}}^H\widehat{\mathbf{A}}_k\overline{\mathbf{w}}}{\overline{\mathbf{w}}^H\widehat{\mathbf{B}}_k\overline{\mathbf{w}}}\right) \quad (13)$$
$$-\lambda\left(\Gamma_k+\rho\ln\left\{\sum\nolimits_{k=1}^{K}\exp\left[\log_2\left(\frac{\overline{\mathbf{w}}^H\widehat{\mathbf{A}}_k\overline{\mathbf{w}}}{\overline{\mathbf{w}}^H\widehat{\mathbf{B}}_k\overline{\mathbf{w}}}\right)^{-\frac{1}{\rho}}\right]\right\}\right)$$
$$-\mu\left(\overline{\gamma}_k+\rho\ln\left\{\sum\nolimits_{k=1}^{K}\exp\left[\log_2\left(\frac{\overline{\mathbf{w}}^H\widehat{\mathbf{A}}_k\overline{\mathbf{w}}}{\overline{\mathbf{w}}^H\mathbf{C}_k\overline{\mathbf{w}}}\right)^{-\frac{1}{\rho}}\right]\right\}\right).$$

The dual problem can be expressed as

$$\min_{\lambda,\mu}\max_{\overline{\mathbf{w}}}\mathcal{L}\left(\overline{\mathbf{w}},\lambda,\mu\right)\ s.t.\ \lambda,\mu\geq 0. \quad (14)$$

Before handling the dual problem (14), we will derive a closed-form solution for $\mathcal{L}\left(\overline{\mathbf{w}}\right)$ with given λ and μ. By calculating the gradient of the Lagrangian function (13) w.r.t. $\overline{\mathbf{w}}$, we can obtain the first-order optimality condition of (12), which is shown in the following lemma.

Lemma 1: The first-order optimality condition of (17) is satisfied when the following holds:

$$\mathbf{M}^{\dagger}\left(\overline{\mathbf{w}}\right)\mathbf{N}\left(\overline{\mathbf{w}}\right)\overline{\mathbf{w}}=\mathcal{L}\left(\overline{\mathbf{w}}\right)\overline{\mathbf{w}}, \quad (15)$$

where $\mathbf{M}\left(\overline{\mathbf{w}}\right)$ and $\mathbf{N}\left(\overline{\mathbf{w}}\right)$ are shown in (16) at the top of this page, and $\mathcal{L}_{\mathrm{num}}\left(\overline{\mathbf{w}}\right)$, $\mathcal{L}_{\mathrm{den}}\left(\overline{\mathbf{w}}\right)$ are the numerator and the denominator of the scalar $\mathcal{L}\left(\overline{\mathbf{w}}\right)$.

Proof: By calculating the gradient of Lagrangian function (13) with respect to $\overline{\mathbf{w}}$ and setting it to zero, we get (15). ■

However, it is still challenging to obtain the closed-form solution to $\overline{\mathbf{w}}$. Thus, we have the following proposition.

Proposition 1: Denoting the fixed point maximizing the objective function of (12) as $\overline{\mathbf{w}}^{\star}$, then $\overline{\mathbf{w}}^{\star}$ must be the leading eigenvector of $\mathbf{M}^{\dagger}\left(\overline{\mathbf{w}}^{\star}\right)\mathbf{N}\left(\overline{\mathbf{w}}^{\star}\right)$ satisfying

$$\mathbf{M}^{\dagger}\left(\overline{\mathbf{w}}^{\star}\right)\mathbf{N}\left(\overline{\mathbf{w}}^{\star}\right)\overline{\mathbf{w}}^{\star}=\lambda_{\max}\overline{\mathbf{w}}^{\star}, \quad (17)$$

where $\lambda_{\max}$ is the maximum eigenvalue. In addition, $\overline{\mathbf{w}}^{\star}$ can be obtained by calculating the following closed-form solution in an iterative manner, i.e.,

$$\overline{\mathbf{w}}^{(i_d+1)}=\sqrt{P_{\max}}\frac{\mathbf{M}^{-1}\left(\overline{\mathbf{w}}^{(i_d)}\right)\mathbf{N}\left(\overline{\mathbf{w}}^{(i_d)}\right)\overline{\mathbf{w}}^{(i_d)}}{\left\|\mathbf{M}^{-1}\left(\overline{\mathbf{w}}^{(i_d)}\right)\mathbf{N}\left(\overline{\mathbf{w}}^{(i_d)}\right)\overline{\mathbf{w}}^{(i_d)}\right\|}, \quad (18)$$

where $\overline{\mathbf{w}}^{(i_d+1)}$ denotes the solution obtained at i_d-th iteration. For the initial point $\overline{\mathbf{w}}^{(0)}$, we can adopt the maximum ratio transmission (MRT). Clearly, the power constraint $\overline{\mathrm{C}}3$ is automatically guaranteed by (18).

Proof: Note that $\overline{\mathbf{w}}$ satisfying (15) is a stationary solution of (12) whose gradient is zero since (15) is the first-order optimality condition. On the other hand, we can observe that the condition (15) is a non-linear eigenvalue problem, i.e., eigenvector-dependent non-linear eigenvalue problem (NEPv) [26], [27], where $\overline{\mathbf{w}}$ is an eigenvector of $\mathbf{M}^{\dagger}\left(\overline{\mathbf{w}}\right)\mathbf{N}\left(\overline{\mathbf{w}}\right)$ corresponding to the eigenvalue $\mathcal{L}\left(\overline{\mathbf{w}}\right)$. Furthermore, $\lambda_{\max}$ is equivalent to $\mathcal{L}\left(\overline{\mathbf{w}}\right)$ in (13). Hence, the leading eigenvector of $\mathbf{M}^{\dagger}\left(\overline{\mathbf{w}}\right)\mathbf{N}\left(\overline{\mathbf{w}}\right)$ can be obtained as the stationary solution of (12), which maximizes the objective function among multiple eigenvectors. Hence, the proof is completed. ■

However, ***Proposition 1*** is executed with fixed λ and μ. Hence, we optimize the optimal λ and μ of the dual problem (14) by using the multi-dimensional bisection search method in [16], which is omitted here for brevity.

B. Optimal Closed-Form Solution for γ_k

After optimizing $\overline{\mathbf{w}}$, we turn to the design of PS ratio γ_k. Note that γ_k is only dependent on the k-th ES's individual utility $R_{\mathrm{ID},k}$, and $R_{\mathrm{ID},k}$ increases as γ_k decreases. Thus, the constraint $\overline{\mathrm{C}}3$ must hold with equality for all ESs at the optimal solution, which is given by

$$\sum\nolimits_{i=1}^{K}\left|\widehat{\mathbf{g}}_k^H\mathbf{w}_i\right|^2=\frac{\overline{\varsigma}_{\max}}{(1-\gamma_k)}. \quad (19)$$

Thus, the optimal closed-form solution for γ_k is obtained as

$$\gamma_k=1-\frac{\overline{\varsigma}_{\max}}{\sum_{i=1}^{K}\left|\widehat{\mathbf{g}}_k^H\mathbf{w}_i\right|^2}. \quad (20)$$

C. Modified Cyclic Coordinate Descent Algorithm for $\boldsymbol{\Xi}_{ka}$

In this subsection, we focus on optimizing the multi-layer RIS's coefficients $\boldsymbol{\Xi}_{ka}$, which only determine the k-th ES's individual achievable rate $R_{\mathrm{ID},k}$. Thus, the designs of RIS's coefficients at each ES are parallel, and formulated as

$$\max_{\boldsymbol{\Xi}_{ka}}\min_{\Delta}\frac{\left|\mathbf{g}_k^H\mathbf{w}_k\right|^2}{\sum_{i\neq k}^{K}\left|\mathbf{g}_k^H\mathbf{w}_i\right|^2+\overline{\sigma}_k^2} \quad (21)$$
$$s.t.\ \mathrm{C}2:\min_{\Delta}\sum\nolimits_{i=1}^{K}\left|\mathbf{g}_k^H\mathbf{w}_i\right|^2\geq\frac{\overline{\varsigma}_{\max}}{(1-\gamma_k)},\mathrm{C}4.$$

Clearly, the above problem is challenging to be solved due to Δ and the non-convexity of both the objective function and constraints. Similar to Section III-A, the discretization method is adopted. By selecting uniformly spaced angles as in (7), we can obtain the robust CSI, which is given by

$$\widehat{\mathbf{H}}_{(k,i),a}=\sum\nolimits_{p=1}^{N_{\mathrm{H1}}N_{\mathrm{E1},k1}}\sum\nolimits_{q=1}^{N_{\mathrm{H2}}N_{\mathrm{E2},k1}}\frac{1}{N_{\mathrm{H}}N_{\mathrm{E},k1}}\widehat{\mathbf{h}}_{(k,i),a}^{(p,q)}\widehat{\mathbf{h}}_{(k,i),a}^{(p,q),H},$$

$$\mathbf{h}_{(k,i),a}^{(p,q),H}=\mathbf{v}_k^H\mathbf{\Omega}_{k,(a+1,A)}\mathbf{B}_{ka}\mathrm{diag}\Big\{\mathbf{\Omega}_{k,(1,a-1)}\mathbf{G}_k^{(p,q)}\mathbf{w}_i\Big\}. \quad (22)$$

Next, after some mathematical manipulations, we can reformulate the subproblem w.r.t $\mathbf{\Xi}_{ka}=\mathrm{diag}\left(\boldsymbol{\xi}_{ka}\right)$ as

$$\max_{\boldsymbol{\xi}_{ka}}\frac{\boldsymbol{\xi}_{ka}^H\widehat{\mathbf{H}}_{(k,k),a}\boldsymbol{\xi}_{ka}}{\boldsymbol{\xi}_{ka}^H\mathbf{R}_{ka}\boldsymbol{\xi}_{ka}+\overline{\sigma}_k^2} \quad (23)$$
$$s.t.\ \overline{\overline{\mathrm{C}}}2:\boldsymbol{\xi}_{ka}^H\mathbf{Q}_{ka}\boldsymbol{\xi}_{ka}\geq\widetilde{\gamma}_k,\overline{\mathrm{C}}4:|[\boldsymbol{\xi}_{ka}]_n|=1,\forall a,n,$$

where $\widetilde{\gamma}_k=\overline{\varsigma}_{\max}/(1-\gamma_k)$, $\mathbf{R}_{ka}=\sum_{i\neq k}^{K}\widehat{\mathbf{H}}_{(k,i),a}$, and $\mathbf{Q}_{ka}=\sum_{i=1}^{K}\widehat{\mathbf{H}}_{(k,i),a}$. Then, to facilitate the derivation of the closed-form solution to (23), we add $\overline{\overline{\mathrm{C}}}2$ into the objective function of (23) with the non-negative Lagrange multiplier τ and utilize the Dinkelbach's method to transform (23) to an equivalent form [28], which is expressed as

$$\max_{\boldsymbol{\xi}_{ka}}f\left(\boldsymbol{\xi}_{ka},\tau,\vartheta\right)=\boldsymbol{\xi}_{ka}^H\mathbf{T}_{ka}\boldsymbol{\xi}_{ka}\ s.t.\ \overline{\mathrm{C}}4, \quad (24)$$

where $\mathbf{T}_{ka}=\widehat{\mathbf{H}}_{(k,k),a}-\vartheta\mathbf{R}_{ka}+\tau\mathbf{Q}_{ka}$, and ϑ is the non-negative Dinkelbach's parameter to be optimized. We observe that problem (24) is NP-hard owing to the multiplicative optimization variables $\boldsymbol{\xi}_{ka}$, τ, and ϑ. Thus, we first propose an efficient algorithm based on the MCCD optimization framework [29] to obtain the closed-form solutions for $\boldsymbol{\xi}_{ka}$ and ϑ. Then, we use the bisection method to search for τ.

As for optimizing $\boldsymbol{\xi}_{ka}$ and ϑ for given τ, we do not optimize overall $\mathbf{p}_{\Xi}$ like the existing methods, while concatenate all the variables into one vector $[\vartheta;\boldsymbol{\xi}_{ka}]$ and then addresses $N_{\mathrm{E},ka}+1$ scalar subproblems upon the block size chosen. Note that we only solve the subproblem w.r.t. $\xi_{ka,i}$ in one iteration, while the remaining variables are updated subsequently such that the closed-form solutions can be obtained, which again results improves CCD implementation over state of the art. To elaborate, we can first expand $f\left(\boldsymbol{\xi}_{ka},\vartheta\right)$ as

$$\begin{aligned}\boldsymbol{\xi}_{ka}^H\mathbf{T}_{ka}\boldsymbol{\xi}_{ka}&=\sum\nolimits_{j=1}^{N_{\mathrm{E},ka}}\sum\nolimits_{i=1}^{N_{\mathrm{E},ka}}\xi_{ka,i}^*T_{ka,(i,j)}\xi_{ka,j}\\&=\sum\nolimits_{i=1}^{N_{\mathrm{E},ka}}\xi_{ka,i}^*T_{ka,(i,i)}\xi_{ka,i}+\sum\nolimits_{j\neq1}^{N_{\mathrm{E},ka}}\sum\nolimits_{i=1}^{N_{\mathrm{E},ka}}\xi_{ka,i}^*T_{ka,(i,j)}\xi_{ka,j}\\&=\sum\nolimits_{i=1}^{N_{\mathrm{E},ka}}T_{ka,(i,i)}+\Re\left(\sum\nolimits_{i=1}^{N_{\mathrm{E},ka}}\xi_{ka,i}^*T_{ka,(i)}\right), \quad (25)\end{aligned}$$

where $T_{ka,(i)}=\sum_{j=1}^{j<i}T_{ka,(i,j)}\xi_{ka,j}+\sum_{j>i}^{N_{\mathrm{E},ka}}T_{ka,(i,j)}\xi_{ka,j}$. Note that the third equality above holds due to the the unit-modulus property and the fact that $\mathbf{T}_{ka}$ is a Hermitian matrix. Hence, we can obtain $N_{\mathrm{E},ka}+1$ scalar subproblems and update them by the following M-CCD algorithm.

$$\begin{cases}\vartheta_1^{(i_d+1)}=o\left(\vartheta,\xi_{ka,1}^{(i_d)},\cdots,\xi_{ka,N_{\mathrm{E},ka}}^{(i_d)}\right),\\ \xi_{ka,1}^{(i_d+1)}=\arg\max\limits_{\xi_{ka,1}\in\mathcal{B}}f\left(\vartheta^{(i_d+1)},\xi_{ka,1},\cdots,\xi_{ka,N_{\mathrm{E},ka}}^{(i_d)}\right),\\ \vdots\\ \vartheta_i^{(i_d+1)}=o\left(\vartheta,\cdots,\xi_{ka,i}^{(i_d)},\cdots,\xi_{ka,N_{\mathrm{E},ka}}^{(i_d)}\right),\\ \xi_{ka,i}^{(i_d+1)}=\arg\max\limits_{\xi_{ka,i}\in\mathcal{B}}f\left(\vartheta^{(i_d+1)},\cdots,\xi_{ka,i},\cdots,\xi_{ka,N_{\mathrm{E},ka}}^{(i_d)}\right),\\ \vdots\\ \vartheta_{N_{\mathrm{E},ka}}^{(i_d+1)}=o\left(\vartheta,\cdots,\xi_{ka,i}^{(i_d+1)},\cdots,\xi_{ka,N_{\mathrm{E},ka}}^{(i_d)}\right),\\ \xi_{ka,N_{\mathrm{E},ka}}^{(i_d+1)}=\arg\max\limits_{\xi_{ka,N_{\mathrm{E},ka}}\in\mathcal{B}}f\left(\vartheta^{(i_d+1)},\xi_{ka,1}^{(i_d+1)},\cdots,\xi_{ka,N_{\mathrm{E},ka}}\right).\end{cases} \quad (26)$$

Given the value for $\boldsymbol{\xi}_{ka}$, ϑ can be solved by the optimal closed-form solution [28]:

$$\vartheta^{(i_d+1)}=o\left(\vartheta,\boldsymbol{\xi}_{ka}^{(i_d)}\right)=\frac{\boldsymbol{\xi}_{ka}^{(i_d),H}\widehat{\mathbf{H}}_{(k,k),a}\boldsymbol{\xi}_{ka}^{(i_d)}}{\boldsymbol{\xi}_{ka}^{(i_d),H}\mathbf{R}_{ka}\boldsymbol{\xi}_{ka}^{(i_d)}+\overline{\sigma}_k^2}. \quad (27)$$

Next, we handle the optimization problem w.r.t. the each component $\xi_{ka,i}$ of $\boldsymbol{\xi}_{ka}$. By ignoring the constant terms in (25), the subproblem w.r.t. $\xi_{ka,i}$ is given by

$$\max_{\xi_{ka,i}}\Re\left(\xi_{ka,i}^*\left(\sum\nolimits_{j=1}^{j<i}T_{ka,(i,j)}\xi_{ka,j}^{(i_d+1)}+\sum\nolimits_{j>i}^{N_{\mathrm{E},ka}}T_{ka,(i,j)}\xi_{ka,j}^{(i_d)}\right)\right)$$
$$s.t.\ \overline{\mathrm{C}}4:\xi_{ka,i}\in\mathcal{B},\forall i. \quad (28)$$

It is evident that (28) admits the closed-form solution of (24):

$$\xi_{ka,i}=\exp\left\{j\arg\left(\sum\nolimits_{j=1}^{j<i}T_{ka,(i,j)}\xi_{ka,j}^{(i_d+1)}+\sum\nolimits_{j>i}^{N_{\mathrm{E},ka}}T_{ka,(i,j)}\xi_{ka,j}^{(i_d)}\right)\right\},\forall i. \quad (29)$$

After finding $\boldsymbol{\xi}_{ka}$ and ϑ, we can optimize the Lagrange multiplier τ by using the bisection search method, which is omitted here for brevity.

D. MMSE Decoder for $\mathbf{v}_{\mathrm{U}}$

In this subsection, we investigate the optimization of the digital decoder $\mathbf{v}_k$ at the k-th ES. According to [30], the linear minimum-mean-square-error (MMSE) detector can be adopted for $\mathbf{v}_k$ as the optimal digital decoder, which can balance between interference and noise at the receiver, i.e.,

$$\mathbf{v}_k=\frac{\left(\sum_{i\neq k}^{K}\widehat{\mathbf{w}}_{(k,i)}\widehat{\mathbf{w}}_{(k,i)}^H+\overline{\sigma}_k^2\mathrm{I}_{N_{\mathrm{D},k}}\right)^{-1}\widehat{\mathbf{w}}_{(k,k)}}{\left\|\left(\sum_{i\neq k}^{K}\widehat{\mathbf{w}}_{(k,i)}\widehat{\mathbf{w}}_{(k,i)}^H+\overline{\sigma}_k^2\mathrm{I}_{N_{\mathrm{D},k}}\right)^{-1}\widehat{\mathbf{w}}_{(k,k)}\right\|}, \quad (30)$$

where $\widehat{\mathbf{w}}_{(k,i)}=\mathbf{\Omega}_{k,(1,A)}\widehat{\mathbf{G}}_k\mathbf{w}_i$.

IV. Simulation Results

In this section, we provide numerical results to evaluate the performance of our proposed architecture and algorithms. We consider a scenario where the HAP with $N_{\mathrm{H}}=8\times8$ antennas serves $K=3$ ESs with $A=2$ layers and $N_{\mathrm{D},k}=2\times2$ Rx antennas. The noise power at ES and energy harvesting circuits are set as $\sigma_k^2=\delta_k^2=-80$ dBm [14], the carrier frequency is 18 GHz [1], and the maximum power at HAP is $P_{\max}=30$ dBm. In addition, the minimum rate threshold Γ_k

and the harvested energy requirement $\varsigma_{\max}$ are set as $\Gamma_k = 1$ bps/Hz and $\varsigma_{\max} = -20$ dBm [14], respectively. The nonlinear energy harvesting model parameters are set to $\alpha = 2.463$, $\beta = 1.635$, and $\varepsilon = 0.826$ [7]. The smoothing parameter is $\rho = 0.1$. Moreover, the CSI uncertainty bound is defined as $\Delta{=}\theta_{\mathrm{U}} - \theta_{\mathrm{L}}$, and the HAP's altitude is D. Here, we compare the following architectures and algorithms:

- **Prop. arch.**: the proposed multi-layer refracting RIS-assisted receiver architecture with A layers having $N_{\mathrm{E},ka} = N_{\mathrm{E}}$ on each layer is adopted for SWIPT, and the proposed scalable robust beamforming optimization framework is utilized to solve problem (5).
- **Digital arch.**: the fully-digital receiver architecture in [16] with $N = AN_{\mathrm{E}}$ Rx antennas is adopted, and MMSE decoder in [30] is used.
- **Sing.-act. arch.**: the single-layer active RIS-aided receiver architecture $N = AN_{\mathrm{E}}$ RIS units is adopted, and the proposed algorithm is applied to obtain $\boldsymbol{\Xi}_k$. To further highlight the superiorities of our proposed architecture, we consider a favorable setting for the single-layer active one, where the maximum amplification factor is set as a constant, while ignoring active RIS's power constraints.
- **Sing.-pass. arch.**: the single-layer passive RIS-aided receiver architecture $N = AN_{\mathrm{E}}$ RIS units is adopted, and the proposed algorithm is applied to obtain $\boldsymbol{\Xi}_k$.
- **SCA-MM scheme**: under the proposed architecture, SCA in [31] and MM in [13] are utilized to handle problem (5).

Fig. 2 presents the transmit (Tx) and receive (Rx) beampattern with different architectures, where $N_{\mathrm{E}} = 6 \times 6$, $\Delta = 2^\circ$, and $D = 20$ km. Here, we focus on investigating the Tx and Rx beampattern of ES 1. As expected, even under the angular uncertainty Δ, the HAP's transmitter can still accurately generate the mainlobe towards the desired ES with SNR value of 0 dB, and simultaneously align the nulls with at least -50 dB with the undesired targets. This demonstrates the validity of the transmit precoder generated by our proposed LogSumExp-dual scheme. In addition, the received ES's SNR acheived by proposed architecture is about 0 dB, while those of the single-layer active and the passive architectures are about -4.2 dB and -10 dB, respectively. This suggests that proposed multi-layer RIS-assisted architecture can amplify the amplitude of the desired signals much more than both the single-layer active and passive ones. Furthermore, as compared with the single-layer passive RIS-receiver whose beampattern is not smooth, those of the proposed and the single-layer active architectures are both smooth, which suggests that the amplitude of the signal penetrating the multi-layer architecture can be partially controlled, thereby leading to additional DoFs.

Fig. 3 illustrates the sum achievable rate versus the number of RIS units at each layer $\sqrt{N_{\mathrm{E}}}$. As we can see, the sum achievable rate increases with increasing N_{E}, especially, when the number of RIS units at each layer increases from 4×4 to 8×8. Furthermore, it can also be observed that, as N_{E} grows, the sum achievable rate of all the benchmark architectures and

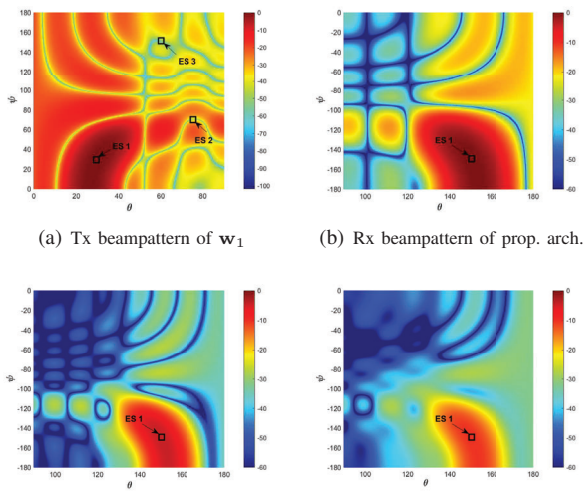

(a) Tx beampattern of $\mathbf{w}_1$ (b) Rx beampattern of prop. arch.

(c) Rx beampattern of sing.-act. arch. (d) Rx beampattern of sing.-pass. arch.

Fig. 2: Beampattern with different architectures.

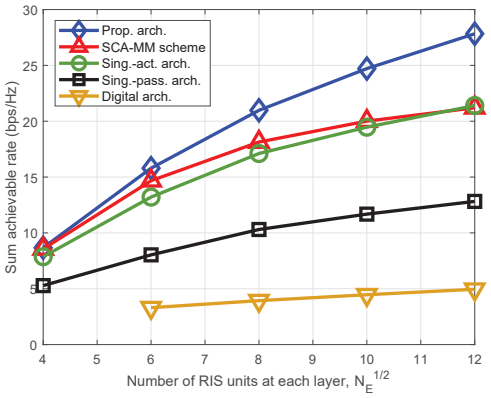

Fig. 3: Sum achievable rate versus $\sqrt{N_{\mathrm{E}}}$.

SCA-MM scheme converges gradually, and the difference in sum achievable rate between the proposed architecture and the benchmarks becomes larger. These results confirm both the superiority and the scalability of our proposed optimization framework as the number of RIS units increases. On the other hand, due to the severe large-scale fading in the HAP-ES link, the digital receiver architecture cannot realize SWIPT when $N_{\mathrm{E}} < 6 \times 6$, while we see the converse for RIS-aided HAP communications. In practice, it is challenging to deploy $N_{\mathrm{Tot}} > 32$ digital antennas at the ES, whereas RIS can facilitate the deployment of large-scale arrays, which indicates that HAP-SWIPT can be realized using RIS.

V. Conclusions

This paper investigated HAP-SWIPT networks with the proposed multi-layer refracting RIS-assisted receiver to overcome the severe large-scale fading and the energy scarcity challenges. Utilizing this architecture and taking the angular CSI imperfection into account, a worst-case sum rate maximization problem was formulated to convey the information

and energy concurrently. To handle the intractable non-convex problem, a scalable robust optimization framework was developed by leveraging the discretization method, LogSumExp-dual scheme, and the M-CCD, which admits semi-closed-form solutions of all optimization variables. Our simulation results showed that the multi-layer RIS-receiver can well overcome the severe "double fading" effect induced by the extreme long-distance HAP links and fully exploit RIS's DoFs for the HAP-SWIPT design.

REFERENCES

[1] Z. Lin, M. Lin, Y. Huang, T. d. Cola, and W.-P. Zhu, "Robust multi-objective beamforming for integrated satellite and high altitude platform network with imperfect channel state information," *IEEE Trans. Signal Process.*, vol. 67, no. 24, pp. 6384–6396, 2019.

[2] K. An, M. Lin, J. Ouyang, and W.-P. Zhu, "Secure transmission in cognitive satellite terrestrial networks," *IEEE J. Sel. Areas Commun.*, vol. 34, no. 11, pp. 3025–3037, 2016.

[3] K. An, M. Lin, T. Liang, J.-B. Wang, J. Wang, Y. Huang, and A. L. Swindlehurst, "Performance analysis of multi-antenna hybrid satellite-terrestrial relay networks in the presence of interference," *IEEE Trans. Commun.*, vol. 63, no. 11, pp. 4390–4404, 2015.

[4] K. An, T. Liang, G. Zheng, X. Yan, Y. Li, and S. Chatzinotas, "Performance limits of cognitive-uplink FSS and terrestrial FS for Ka-band," *IEEE Trans. Aerosp. Electron. Syst.*, vol. 55, no. 5, pp. 2604–2611, 2019.

[5] K. An and T. Liang, "Hybrid satellite-terrestrial relay networks with adaptive transmission," *IEEE Trans. Veh. Technol.*, vol. 68, no. 12, pp. 12 448–12 452, 2019.

[6] Y. Alsaba, S. K. A. Rahim, and C. Y. Leow, "Beamforming in wireless energy harvesting communications systems: A survey," *IEEE Commun. Surv. Tuts.*, vol. 20, no. 2, pp. 1329–1360, 2018.

[7] Y. Chen, N. Zhao, and M.-S. Alouini, "Wireless energy harvesting using signals from multiple fading channels," *IEEE Trans. Commun.*, vol. 65, no. 11, pp. 5027–5039, 2017.

[8] W. Feng, J. Tang, Y. Yu, J. Song, N. Zhao, G. Chen, K.-K. Wong, and J. Chambers, "UAV-enabled SWIPT in IoT networks for emergency communications," *IEEE Wireless Commun.*, vol. 27, no. 5, pp. 140–147, 2020.

[9] Q. Wu and R. Zhang, "Beamforming optimization for wireless network aided by intelligent reflecting surface with discrete phase shifts," *IEEE Trans. Commun.*, vol. 68, no. 3, pp. 1838–1851, 2020.

[10] ——, "Intelligent reflecting surface enhanced wireless network via joint active and passive beamforming," *IEEE Trans. Wireless Commun.*, vol. 18, no. 11, pp. 5394–5409, 2019.

[11] Z. Lin, H. Niu, K. An, and et al, "Refracting RIS-aided hybrid satellite-terrestrial relay networks: Joint beamforming design and optimization," *IEEE Trans. Aerosp. Electron. Syst.*, vol. 58, no. 4, pp. 3717–3724, 2022.

[12] Y. Sun, K. An, J. Luo, Y. Zhu, G. Zheng, and S. Chatzinotas, "Intelligent reflecting surface enhanced secure transmission against both jamming and eavesdropping attacks," *IEEE Trans. Veh. Technol.*, vol. 70, no. 10, pp. 11 017–11 022, 2021.

[13] C. Pan, H. Ren, K. Wang, M. Elkashlan, A. Nallanathan, J. Wang, and L. Hanzo, "Intelligent reflecting surface aided MIMO broadcasting for simultaneous wireless information and power transfer," *IEEE J. Sel. Areas Commun.*, vol. 38, no. 8, pp. 1719–1734, 2020.

[14] S. Zargari, A. Hakimi, C. Tellambura, and S. Herath, "Multiuser MISO PS-SWIPT systems: Active or passive RIS?" *IEEE Wireless Commun. Lett.*, vol. 11, no. 9, pp. 1920–1924, 2022.

[15] Y. Sun, Y. Zhu, K. An, G. Zheng, S. Chatzinotas, K.-K. Wong, and P. Liu, "Robust design for RIS-assisted anti-jamming communications with imperfect angular information: A game-theoretic perspective," *IEEE Trans. Veh. Technol.*, vol. 71, no. 7, pp. 7967–7972, 2022.

[16] Y. Sun, K. An, Y. Zhu, G. Zheng, K.-K. Wong, S. Chatzinotas, H. Yin, and P. Liu, "RIS-assisted robust hybrid beamforming against simultaneous jamming and eavesdropping attacks," *IEEE Trans. Wireless Commun.*, vol. 21, no. 11, pp. 9212–9231, 2022.

[17] Y. Sun, K. An, C. Li, Z. Lin, H. Niu, D. W. K. Ng, J. Wang, and N. Al-Dhahir, "Joint transmissive and reflective RIS-aided secure MIMO systems design under spatially-correlated angular uncertainty and coupled PSEs," *IEEE Trans. Inf. Forensics Security*, vol. 18, pp. 3606–3621, 2023.

[18] Y. Sun, K. An, Y. Zhu, G. Zheng, K.-K. Wong, S. Chatzinotas, D. W. K. Ng, and D. Guan, "Energy-efficient hybrid beamforming for multilayer RIS-assisted secure integrated terrestrial-aerial networks," *IEEE Trans. Commun.*, vol. 70, no. 6, pp. 4189–4210, 2022.

[19] Y. Sun, K. An, J. Luo, and et al, "Outage constrained robust beamforming optimization for multiuser IRS-assisted anti-jamming communications with incomplete information," *IEEE Inter. Things J.*, vol. 9, no. 15, pp. 13 298–13 314, 2022.

[20] C. Pan, G. Zhou, K. Zhi, S. Hong, T. Wu, Y. Pan, H. Ren, M. D. Renzo, A. Lee Swindlehurst, R. Zhang, and A. Y. Zhang, "An overview of signal processing techniques for RIS/IRS-aided wireless systems," *IEEE J. Sel. Topics Signal Process.*, vol. 16, no. 5, pp. 883–917, 2022.

[21] Z. Lin, K. An, H. Niu, Y. Hu, S. Chatzinotas, G. Zheng, and J. Wang, "slnr," *IEEE Trans. Aerosp. Electron. Syst.*

[22] W. Lu, K. An, and T. Liang, "Robust beamforming design for sum secrecy rate maximization in multibeam satellite systems," *IEEE Trans. Aerosp. Electron. Syst.*, vol. 55, no. 3, pp. 1568–1572, 2019.

[23] W. Lu, K. An, T. Liang, G. Zheng, and S. Chatzinotas, "Secure energy efficiency maximization in cognitive satellite-terrestrial networks," *IEEE Syst. J.*, vol. 15, no. 2, pp. 2382–2385, 2021.

[24] W. Lu, K. An, T. Liang, and X. Yan, "Robust beamforming in multibeam satellite systems with non-orthogonal multiple access," *IEEE Wireless Commun. Lett.*, vol. 9, no. 11, pp. 1889–1893, 2020.

[25] Z. Lin, M. Lin, B. Champagne, W.-P. Zhu, and N. Al-Dhahir, "Secrecy-energy efficient hybrid beamforming for satellite-terrestrial integrated networks," *IEEE Trans. Commun.*, vol. 69, no. 9, pp. 6345–6360, 2021.

[26] E. Choi, M. Oh, J. Choi, J. Park, N. Lee, and N. Al-Dhahir, "Joint precoding and artificial noise design for MU-MIMO wiretap channels," *IEEE Trans. Commun.*, pp. 1–1, 2022.

[27] Y. Cai, L.-H. Zhang, Z. Bai, and R.-C. Li, "On an eigenvector-dependent nonlinear eigenvalue problem," *SIAM J. Matrix Anal. Appl.*, vol. 39, no. 3, pp. 1360–1382, 2018.

[28] K. Shen and W. Yu, "Fractional programming for communication systems-Part I: Power control and beamforming," *IEEE Trans. Signal Process.*, vol. 66, no. 10, pp. 2616–2630, 2018.

[29] A. Arora, C. G. Tsinos, M. R. B. Shankar, S. Chatzinotas, and B. Ottersten, "Efficient algorithms for constant-modulus analog beamforming," *IEEE Trans. Signal Process.*, vol. 70, pp. 756–771, 2022.

[30] V. Wong, R. Schober, D. W. K. Ng, and L. C. Wang, "Key technologies for 5G wireless systems," *Cambridge University Press*, 2017.

[31] Z. Lin, M. Lin, J. Ouyang, W.-P. Zhu, A. D. Panagopoulos, and M.-S. Alouini, "Robust secure beamforming for multibeam satellite communication systems," *IEEE Trans. Veh. Technol.*, vol. 68, no. 6, pp. 6202–6206, 2019.